HEFAT2007
5th International Conference on Heat Transfer, Fluid Mechanics and Thermodynamics
1-4 July 2007, Sun City, South Africa
Paper number: CM1

LAMINAR NATURAL CONVECTION INSIDE SHALLOW AND SLENDER RECTANGULAR CAVITIES DISCRETELY HEATED AT THE BOTTOM AND COOLED AT THE SIDES

M. Corcione* and E. Habib
*Author for correspondence
Dipartimento di Fisica Tecnica, University of Rome "La Sapienza"
via Eudossiana, 18 – 00184 Rome, Italy
e-mail: massimo.corcione@uniroma1.it

ABSTRACT

Steady laminar natural convection in air-filled rectangular enclosures, both shallow and slender, partially heated at the bottom wall and cooled at both sides, is studied numerically. SIMPLE-C algorithm is employed for the solution of the mass, momentum, and energy transfer equations. Simulations are performed for height-to-width aspect ratios of the cavity from 0.2 to 5, Rayleigh numbers based on the height of the cavity from 10^2 to 10^7, and values of the heated fraction of the bottom endwall between 0.2 and 1.

INTRODUCTION

Natural convection inside rectangular enclosures has been extensively studied both experimentally and numerically, owing to its importance in many engineering applications, e.g., heat transfer in buildings, solar energy collection, heat removal in electronics, and cooling of nuclear reactors, to name a few.

Most of the papers on this topic are related to unidirectional heat flows, but real-life systems are more usually characterized by multi-directional heat flows, i.e., neither simply horizontal nor vertical. Moreover, in many practical cases mixed thermal conditions on the same boundary wall may also be encountered, which is, e.g., what happens when a boundary wall is only partially heated or cooled. Focusing the interest on the heating-from-below situation with the assumption of isothermal walls, studies on this topic were conducted by Sezai and Mohamad [1], Aydin and Yang [2], Deng et al. [3], Calcagni et al. [4], and Oosthuizen and Paul [5], in which a specific reference to the cooling of electronic components is made. However, none of these authors either treated the case of tall cavity or developed a correlating equation for predicting the amount of heat transferred across the enclosure.

In this background, the aim of the present paper is to carry out a study of natural convection heat and momentum transfer inside air-filled, rectangular cavities, both shallow and slender, partially heated at the bottom endwall, and cooled at both sidewalls. In particular, the heated boundary surface, which is considered to be symmetric about the vertical midplane of the enclosure, is assumed to be kept at uniform temperature, whilst the remaining parts of the bottom endwall, as well as the top endwall, are assumed to be perfectly insulated.

The study is conducted numerically under the assumption of two-dimensional laminar flow. Simulations are performed for different values of the Rayleigh number based on the height of the cavity in the range between 10^2 and 10^7, the heated fraction of the bottom endwall in the range between 0.2 and 1, and the height-to-width aspect ratio of the cavity from 0.2 to 5, whose effects on the flow pattern, the temperature distribution, and the heat transfer rates, are analyzed and discussed. Heat transfer dimensionless correlating equations are also proposed.

MATHEMATICAL FORMULATION

An air-filled, rectangular enclosure of height H and width W is partially heated at the bottom endwall, and cooled at both sidewalls. The central portion of the bottom wall, of length L, is heated at uniform temperature T_H, while both sides are cooled at temperature T_C. The remaining parts of the bottom endwall, as well as the top endwall, are considered perfectly insulated, as sketched in Fig. 1, where the coordinate system adopted is also represented.

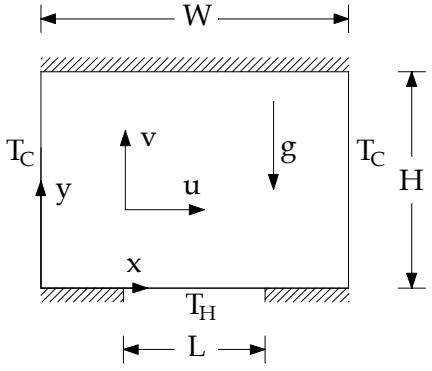

Figure 1 – Sketch of the geometry and coordinate system

The buoyancy-driven flow is considered two-dimensional and laminar. The fluid is assumed incompressible, with constant physical properties and negligible viscous dissipation and pressure work. The buoyancy effects upon momentum transfer are taken into account through the Boussinesq approximation.

Once the above assumptions are used into the conservation equations of mass, momentum and energy, and the following dimensionless variables are introduced:

$$X = \frac{x}{H} \qquad Y = \frac{y}{H} \qquad \tau = \frac{t}{\left(H^2/\nu\right)} \tag{1}$$

$$U = \frac{u}{\left(\nu/H\right)} \qquad V = \frac{v}{\left(\nu/H\right)} \qquad P = \frac{p + \rho_0 g y}{\rho\left(\nu/H\right)^2} \tag{2}$$

$$\theta = \frac{\left(T - T_0\right)}{\left(T_H - T_C\right)} \quad \text{with} \quad T_0 = \frac{LT_H + 2HT_C}{L + 2H} \tag{3}$$

the following set of governing equations is obtained:

$$\frac{\partial U}{\partial X} + \frac{\partial V}{\partial Y} = 0 \tag{4}$$

$$\frac{\partial U}{\partial \tau} + U\frac{\partial U}{\partial X} + V\frac{\partial U}{\partial Y} = -\frac{\partial P}{\partial X} + \left(\frac{\partial^2 U}{\partial X^2} + \frac{\partial^2 U}{\partial Y^2}\right) \tag{5}$$

$$\frac{\partial V}{\partial \tau} + U\frac{\partial V}{\partial X} + V\frac{\partial V}{\partial Y} = -\frac{\partial P}{\partial Y} + \left(\frac{\partial^2 V}{\partial X^2} + \frac{\partial^2 V}{\partial Y^2}\right) + \frac{Ra}{Pr}\theta \tag{6}$$

$$\frac{\partial \theta}{\partial \tau} + U\frac{\partial \theta}{\partial X} + V\frac{\partial \theta}{\partial Y} = \frac{1}{Pr}\left(\frac{\partial^2 \theta}{\partial X^2} + \frac{\partial^2 \theta}{\partial Y^2}\right) \tag{7}$$

Here x and y are the horizontal and vertical coordinates, respectively, with the corresponding velocity components u and v; t is the time; T is the temperature; T_0 is the surface mean temperature; p is the pressure; ρ is the density; ρ_0 is the density at the reference temperature T_0; g is the acceleration of gravity; ν is the kinematic viscosity; Pr is the Prandtl number; and Ra is the Rayleigh number defined as:

$$Ra = \frac{g\beta(T_H - T_C)H^3}{\nu^2}Pr \tag{8}$$

Other parameters which enter into this study are:
(a) the heated fraction of the bottom endwall

$$E = \frac{L}{W} \qquad 0.2 \le E \le 1 \tag{9}$$

(b) the height-to-width aspect ratio of the enclosure

$$A = \frac{H}{W} \qquad 1/5 \le A \le 5 \tag{10}$$

On account of eqs. (3), (9), and (10), it results:

$$\theta = \frac{2A\left(T - T_C\right) - E\left(T_H - T\right)}{\left(2A + E\right)\left(T_H - T_C\right)} \tag{11}$$

and the following relations for the dimensionless temperatures θ_H and θ_C of the heated and cooled boundary surfaces of the enclosure may then be derived:

$$\theta_H = \frac{2A}{2A + E} \tag{12}$$

$$\theta_C = -\frac{E}{2A + E} = \theta_H - 1 \tag{13}$$

The boundary conditions assumed are the no-slip condition U = V = 0 at the four boundary walls, and $\theta = \theta_H$ and $\theta = \theta_C$ at the heated and cooled boundaries, respectively.

The initial conditions assumed are fluid at rest and uniform temperature $\theta = 0$ across the whole cavity.

COMPUTATIONAL PROCEDURE

The set of governing equations (4)–(7) with the boundary conditions stated above is solved through a control-volume formulation of the finite-difference method. The pressure-velocity coupling is handled by the SIMPLE-C algorithm by Van Doormaal and Raithby [6]. The advection fluxes across the surfaces of the control volumes are evaluated by the QUICK discretization scheme by Leonard [7]. A second-order backward scheme is then used for time stepping.

Starting from assigned initial fields of the dependent variables, at each time-step the discretized governing equations are solved iteratively through a line-by-line application of the Thomas algorithm, enforcing under-relaxation for convergence.

The computational spatial domain is covered with a non-uniform grid, having a concentration of grid lines near the boundary walls and both ends of the heated bottom surface, and a uniform spacing across the remainder interior of the cavity. Time discretization is chosen uniform.

Within each time step, the spatial solution is considered to be fully converged when the maximum absolute values of both the mass source and the percent changes of the dependent variables at any grid-node from iteration to iteration are smaller than prescribed values, i.e., 10^{-4} and 10^{-5}, respectively. Time-integration is stopped once an asymptotic steady solution is reached. This means that the simulation procedure ends when the percent difference between the incoming and outgoing heat transfer rates, and the percent changes of the time-derivatives of the dependent variables at any grid-node from time-step to time-step, are smaller than prescribed values, i.e., 10^{-6} and 10^{-7}, respectively.

After convergence is attained, the average Nusselt numbers Nu_H and Nu_C of the heated and cooled boundaries, respectively, are calculated:

$$Nu_H = \frac{h_H H}{k} = \frac{Q_{in} H}{kL\left(T_H - T_C\right)} =$$

$$= \frac{A}{E}\cdot\frac{Q_{in}}{k\left(T_H - T_C\right)} = -\frac{A}{E}\int_{(1-E)/2A}^{(1+E)/2A}\left.\frac{\partial\theta}{\partial Y}\right|_{Y=0} dX \tag{14}$$

$$Nu_C = \frac{h_C H}{k} = \frac{Q_{out} H}{2kH(T_C - T_H)} = \frac{1}{2} \cdot \frac{Q_{out}}{k(T_C - T_H)} =$$

$$= \frac{1}{2}\int_0^1 \left.\frac{\partial\theta}{\partial X}\right|_{X=0} dY - \frac{1}{2}\int_0^1 \left.\frac{\partial\theta}{\partial X}\right|_{X=1/A} dY \qquad (15)$$

where h_H and h_C are the average coefficients of convection of the heated and cooled boundary surfaces, respectively, and Q_{in} and Q_{out} are the overall incoming and outgoing heat transfer rates, respectively. The temperature gradients at any boundary surface are evaluated through a second-order profile among each wall-node and the next corresponding two fluid-nodes.

Of course, since at steady-state the incoming and outgoing heat transfer rates must be the same, i.e., $Q_{in} = -Q_{out} = Q$, at steady-state the following relationship between Nu_H and Nu_C holds:

$$\frac{Nu_H}{Nu_C} = \frac{2A}{E} \qquad (16)$$

Tests on the dependence of the results on both grid-size and time-step have been performed for several combinations of the independent variables A, E, and Ra. The optimal grid-size and time-step used for computations, which represent a good compromise between solution accuracy and computational time required, are such that further refinements do not yield for noticeable modifications neither in the heat transfer rates nor in the flow field, that is, the percent difference between the first and the second members of eq. (16), and the percent changes of the maximum and minimum values of the vertical velocity component on the horizontal midplane of the enclosure, must be smaller than prescribed accuracy values, i.e., 1% and 2–4%, respectively. Typically, the number of nodal points lies in the range between 30×30 and 80×400, and the time stepping lie in the range between 10^{-3} and 10^{-6}.

Furthermore, in order to validate the numerical code used for the present study, the steady-state solutions obtained for $\tau \to \infty$ in a square cavity with differentially heated sidewalls and adiabatic top and bottom endwalls for Rayleigh numbers from 10^3 to 10^6, have been compared with the benchmark results of de Vahl Davis [8], obtained by a standard finite-difference method used to solve the stream function-vorticity formulation of the governing equations. In particular, the average Nusselt numbers throughout the cavity as well as the maximum horizontal and vertical velocity components on the vertical and horizontal midplanes, respectively, are within 1% of the benchmark data, as indicated in Table 1, where other reference solutions derived through finite-volume methods (column FV) are also reported (i.e., the solutions obtained by Mahdi and Kinney [9], for Ra = 10^3, and by Hortmann et al. [10], for Ra = 10^4 to 10^6). It seems worth noticing that our dimensionless velocity results have been multiplied by the Prandtl number before being inserted in Table 1, so as to account for the choice of the ratio between kinematic viscosity and characteristic length of the cavity as scale factor for the velocity, instead of the ratio between thermal diffusivity and characteristic length, used by de Vahl Davis [8].

Table 1 – Comparison of thermally-driven square cavity solutions

Quantities	Benchmark [8]	Present	FV [9]-[10]
		Ra = 10^3	
U_{max}	3.649	3.654	3.649
V_{max}	3.697	3.708	3.690
Nu_{av}	1.118	1.116	1.113
		Ra = 10^4	
U_{max}	16.178	16.242	16.180
V_{max}	19.617	19.714	19.629
Nu_{av}	2.243	2.254	2.244
		Ra = 10^5	
U_{max}	34.722	35.008	34.739
V_{max}	68.590	68.109	68.639
Nu_{av}	4.519	4.506	4.521
		Ra = 10^6	
U_{max}	64.630	65.226	64.836
V_{max}	219.360	221.598	220.461
Nu_{av}	8.800	8.879	8.825

RESULTS AND DISCUSSION

Numerical simulations are performed for Pr = 0.71, which corresponds to air, and different values of (a) the height-to-width aspect ratio of the enclosure A in the range between 0.2 and 5, (b) the heated fraction of the bottom endwall E in the range between 0.2 and 1, and (c) the Rayleigh number Ra based on the height of the cavity in the range between 10^3 and 10^7.

A selection of local results is presented in Figs. 2–7, where isotherm and streamline contours are plotted for different sets of values of A, E, and Ra, in order to highlight the effects of any independent parameter on the flow and temperature fields. In Figs. 2–4 the Rayleigh number is maintained at 10^5, so as to point out the effects of E for different values of A. In Figs. 5–7 the heated fraction of the bottom endwall is maintained at 0.4, so as to point out the effects of Ra for different values of A.

In the isotherm plots (Figs. 2a–7a), the contours correspond to equispaced values of the dimensionless temperature θ in the range from θ_C to $\theta_H = 1 + \theta_C$. In the streamline plots (Figs. 2b–7b), the contours correspond to equispaced values of the normalized dimensionless stream function $|\Psi|/|\Psi|_{max}$ in the range from 0 to 1, where Ψ is defined through $U = \partial\Psi/\partial Y$ and $V = -\partial\Psi/\partial X$.

It may be seen that, owing to the symmetry of the boundary conditions, the resulting fields are symmetric about the vertical midplane of the cavity. The flow field consists of two counter-rotating cells, each one located in one half of the cavity, which originate from the rising of the hot fluid in the middle of the enclosure and its descent along both sidewalls. The intensity of the fluid motion, which depends on the relative importance between buoyancy force and viscous force, increases as: (a) the heated fraction of the bottom endwall E increases, see Figs. 2–4; (b) the Rayleigh number Ra increases, see Figs. 5–7; and (c) the height-to-width aspect ratio A decreases, see Figs. 2–4 and Figs. 5–7.

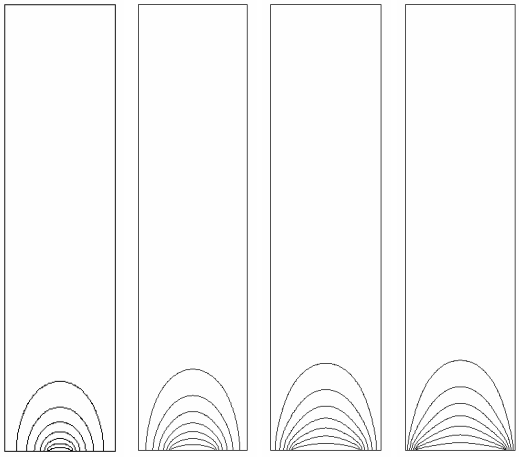

Figure 2a – Isotherms for Ra = 10^5, A = 4 and E = 0.2, 0.4, 0.6, 0.8

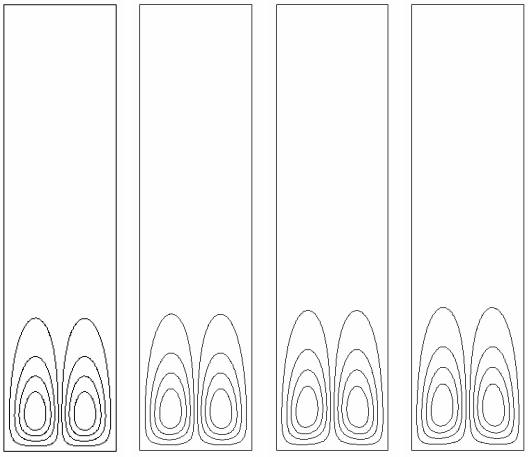

Figure 2b – Streamlines for Ra = 10^5, A = 4 and E = 0.2, 0.4, 0.6, 0.8

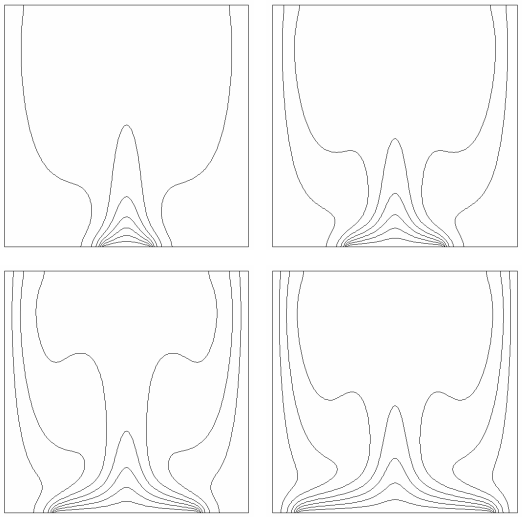

Figure 3a – Isotherms for Ra = 10^5, A = 1 and E = 0.2, 0.4, 0.6, 0.8

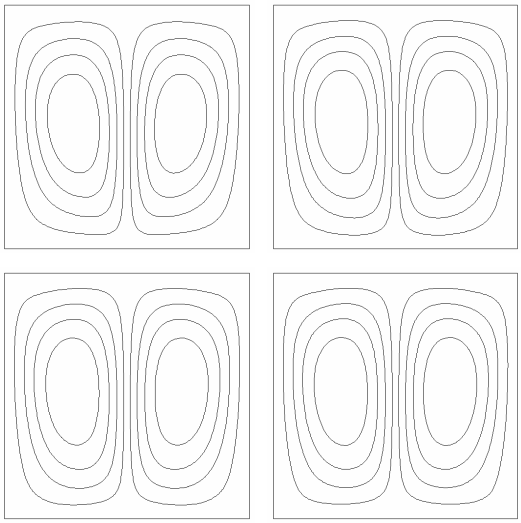

Figure 3b – Streamlines for Ra = 10^5, A = 1 and E = 0.2, 0.4, 0.6, 0.8

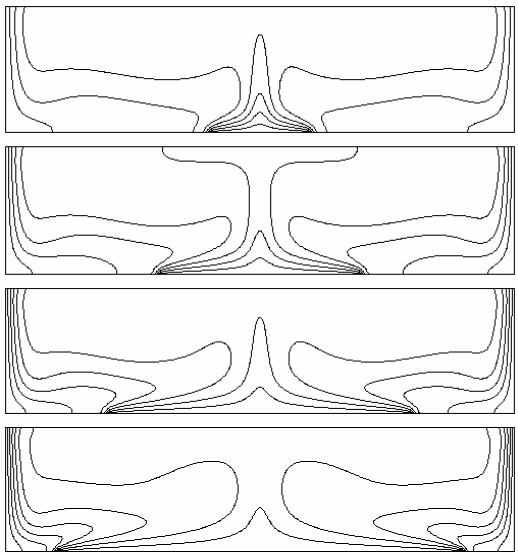

Figure 4a – Isotherms for Ra = 10^5, A = 0.25 and E = 0.2, 0.4, 0.6, 0.8

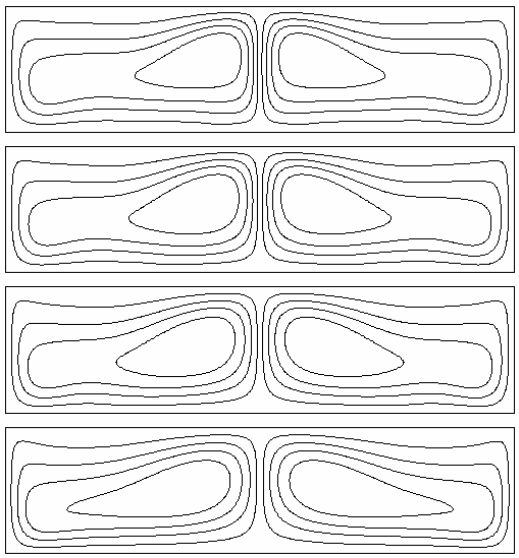

Figure 4b – Streamlines for Ra = 10^5, A = 0.25 and E = 0.2, 0.4, 0.6, 0.8

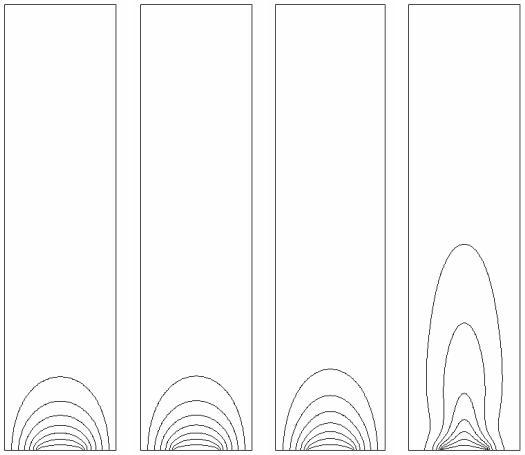

Figure 5a – Isotherms for A = 4, E = 0.4 and Ra = 10^3, 10^4, 10^5, 10^6

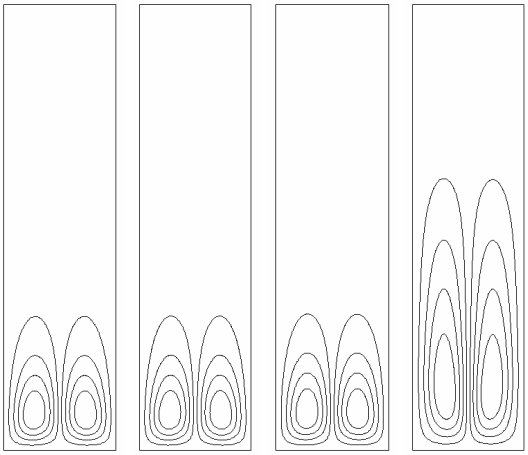

Figure 5b – Streamlines for A = 4, E = 0.4 and Ra = 10^3, 10^4, 10^5, 10^6

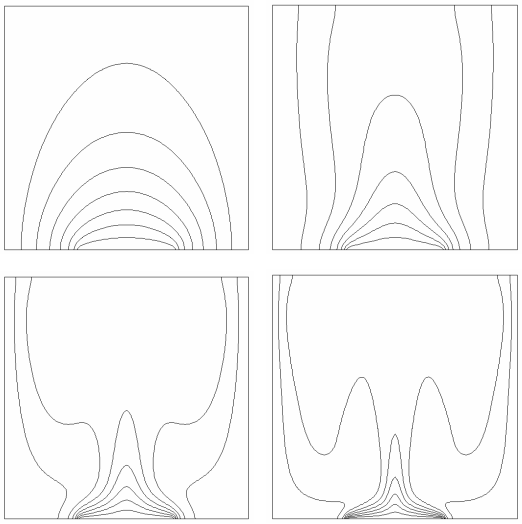

Figure 6a – Isotherms for A = 1, E = 0.4 and Ra = 10^3, 10^4, 10^5, 10^6

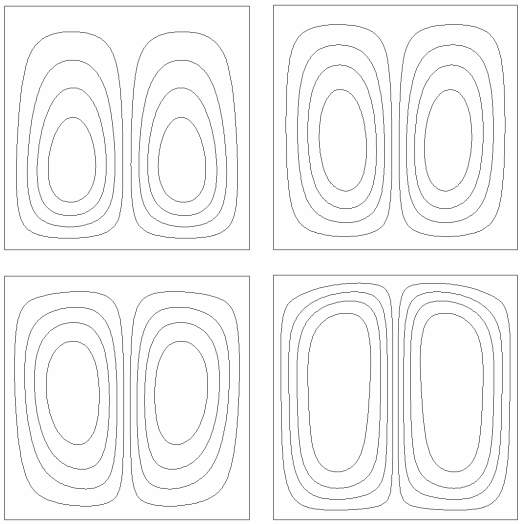

Figure 6b – Streamlines for A = 1, E = 0.4 and Ra = 10^3, 10^4, 10^5, 10^6

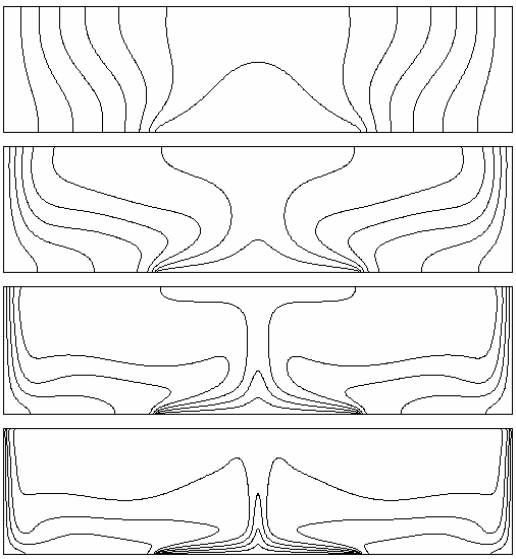

Figure 7a – Isotherms for A = 0.25, E = 0.4 and Ra = 10^3, 10^4, 10^5, 10^6

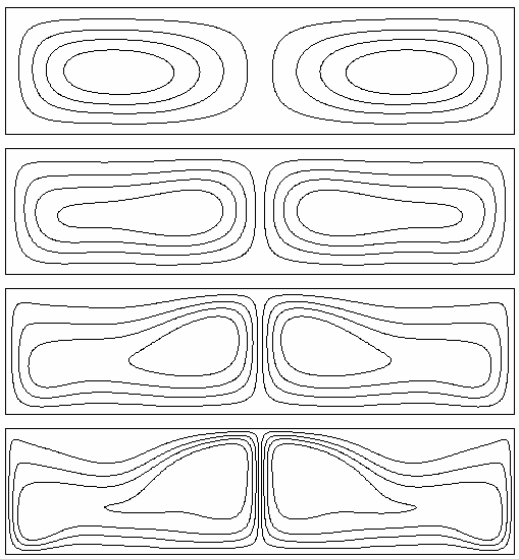

Figure 7b – Streamlines for A = 0.25, E = 0.4 and Ra = 10^3, 10^4, 10^5, 10^6

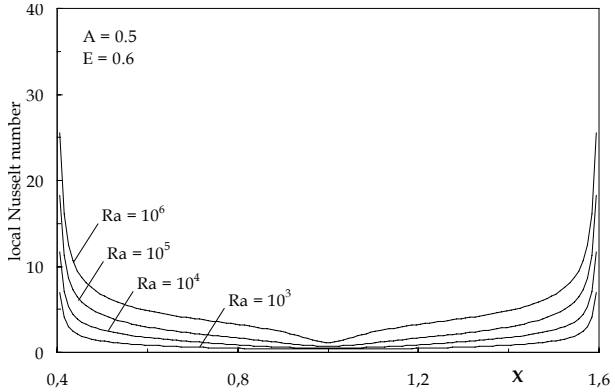

Figure 8 – Distributions of the local Nusselt number on the bottom wall for A = 0.5, E = 0.6 and different values of Ra

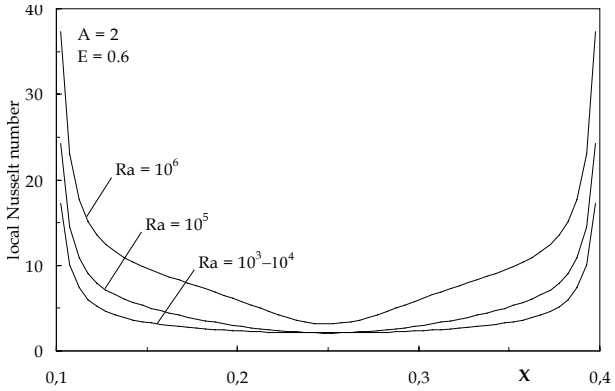

Figure 9 – Distributions of the local Nusselt number on the bottom wall for A = 2, E = 0.6 and different values of Ra

As the intensity of the fluid motion inside the enclosure increases, the cores of the two cells move upwards, and the isotherms become progressively more distorted with respect to the distribution typical of pure conduction, more warped around the two centers of rotation, and more compressed towards the boundary walls of the cavity, which implies an increase in the temperature gradients, and, correspondingly, in the heat transfer rates. The local temperature gradient on the bottom endwall, and then the local Nusselt number $[-(\partial\theta/\partial Y)]_0$, is higher at both ends of the heated surface, decreasing steeply as one moves towards the vertical midplane of the cavity, where it reaches a minimum, as shown in Figs. 8 and 9 for E = 0.6, Ra = 10^3 to 10^6, and A = 0.5 and 2, respectively.

As far as the overall results are concerned, the heat transfer performance of the whole cavity is expressed in terms of Nu_C, which is considered more appropriate to this purpose than Nu_H. In fact, as said above, once Ra is assigned, the amount Q of heat transferred across the enclosure increases with increasing the heated fraction E of the bottom endwall, and decreasing the aspect ratio A of the cavity. Correspondingly, a Nusselt number which would represent the thermal behavior of the cavity "at a glance" should increase with increasing E and decreasing A. On the other hand, according to eq. (14), it is $Nu_H \sim Q \times A/E$. This means that, once A is assigned, Nu_H may either increase or decrease with increasing E, depending on whether $\partial Q/\partial E$ is positive or negative. Similarly, given the value of E, Nu_H may either decrease or increase with increasing A, depending on whether $\partial Q/\partial(1/A)$ is negative or positive. Actually, from Figs. 8 and 9, and from eq. (14), it results that Nu_H increases with A, instead of decreasing as would be preferable.

In contrast, from eq. (15) it results $Nu_C \sim Q$, which implies that Nu_C unequivocally increases with E and decreases with A.

For this same reason, the effectiveness of heat removal from the bottom wall is described better through a Nusselt number Nu* which uses L instead of H as characteristic length:

$$Nu^* = \frac{h_H L}{k} = \frac{Q_{in} L}{kL(T_H - T_C)} = \frac{E}{A} Nu_H = 2Nu_C \qquad (17)$$

Distributions of Nu*, and then, according to eq. (17), also of $Nu_C = 0.5Nu^*$, are plotted against the Rayleigh number Ra in Figs. 10 and 11, for A = 0.5 and E from 0.2 to 0.8, and for E = 0.6 and A from 0.25 to 4, respectively, where a good agreement with the results of Aydin and Yang [2] for A = 1 may be noticed.

As regards the development of a correlation among Nu* and the independent variables A, E, and Ra, the Rayleigh number Ra_L based on the length L of the heated portion of the bottom endwall is introduced:

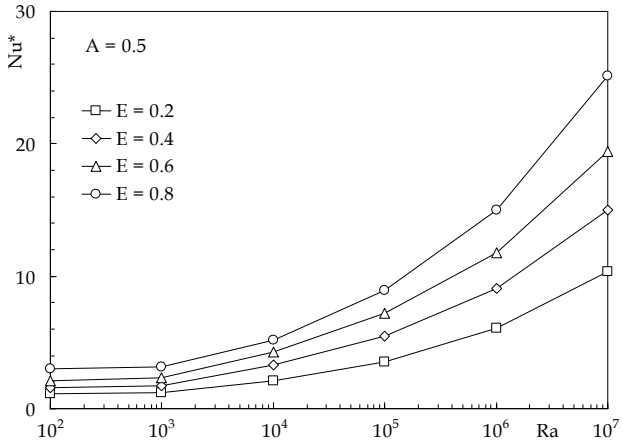

Figure 10 – Distributions of Nu* vs. Ra for A = 0.5 and different values of the heated fraction of the bottom endwall E

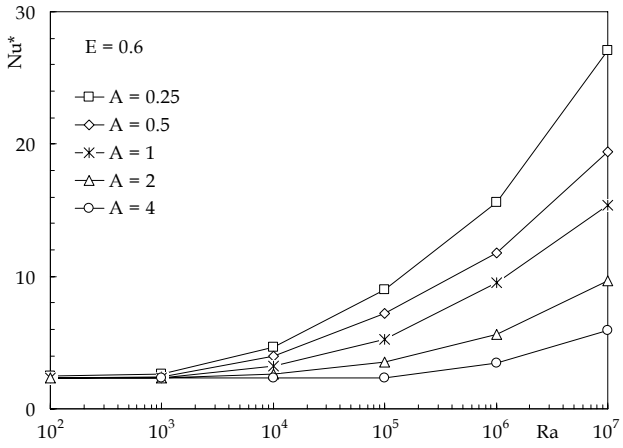

Figure 11 – Distributions of Nu* vs. Ra for E = 0.6 and different values of the height-to-width aspect ratio of the enclosure A

$$Ra_L = \frac{g\beta(T_H - T_C)L^3}{\nu^2} Pr \qquad (18)$$

In fact, on account of eqs. (8)–(10) and (18), it follows:

$$Ra_L = Ra\left(\frac{E}{A}\right)^3 \qquad (19)$$

Therefore, Ra_L increases with Ra and E and decreases with A, which is exactly what happens for the heat transfer rate across the cavity, as discussed above, thus implying that Ra_L might be used for a more synthetic first-approach "description" of the problem treated here.

Indeed, the numerical results obtained for Nu*, and then for $Nu_C = 0.5Nu^*$, can be expressed by the following semi-empiric correlating equations:

✓ slender geometry

$$Nu^* = 0.29\, Ra_L^{0.222} \qquad (20)$$

for $1 \le A \le 5$, $0.2 \le E \le 0.8$, and $10^3 < Ra \le 10^7$, with a 6.13% standard deviation of error, and a ±10% range of error with a 88% level of confidence, as shown in Fig. 12;

✓ shallow geometry

$$Nu^* = 0.22\, Ra_L^{F(A)} \quad \text{with} \quad F(A) = 0.215 + 0.035A \qquad (21)$$

for $0.25 \le A \le 1$, $0.2 \le E \le 0.8$, and $10^3 < Ra \le 10^7$, with a 6.38% standard deviation of error, and a ±10% range of error with a 87.5% level of confidence, as shown in Fig. 13.

CONCLUSIONS

Natural convection inside air-filled, rectangular cavities, both shallow and slender, discretely heated at the bottom and cooled at both sides, has been studied numerically, for different values of the height-to-width aspect ratio of the enclosure, the heated fraction of the bottom wall, and the Rayleigh number based on the height of the enclosure.

It has been found that, due to the symmetry of the boundary conditions applied, the resulting flow field consists of two roll-cells symmetric about the vertical midplane of the enclosure.

The intensity of the fluid motion, and then the consequent heat transfer rate across the enclosure, increases with increasing the heated fraction of the bottom endwall and the Rayleigh number, while decreasing as the aspect ratio of the cavity increases.

Finally, the effectiveness of heat removal from the bottom wall is described better through a Nusselt number based on the length of the heated portion of the bottom wall, rather than on the same characteristic length used in the Rayleigh number, i.e., the height of the enclosure.

NOMENCLATURE

A height-to-width aspect ratio of the enclosure
E heated fraction of the bottom endwall
g gravitational acceleration
H height of the enclosure
h average coefficient of convection

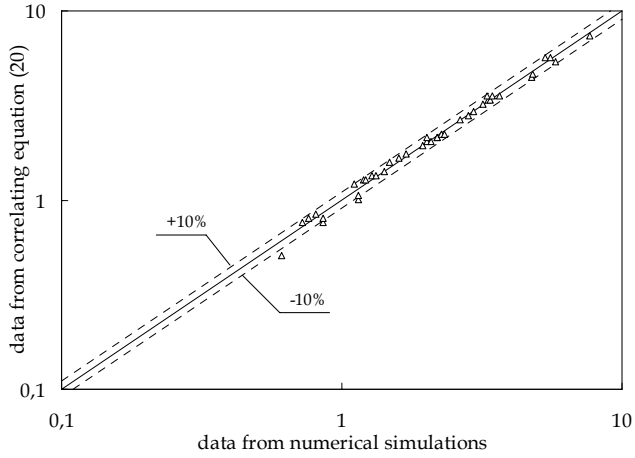

Figure 12 –Nu* from eq. (20) vs. Nu* from numerical simulations

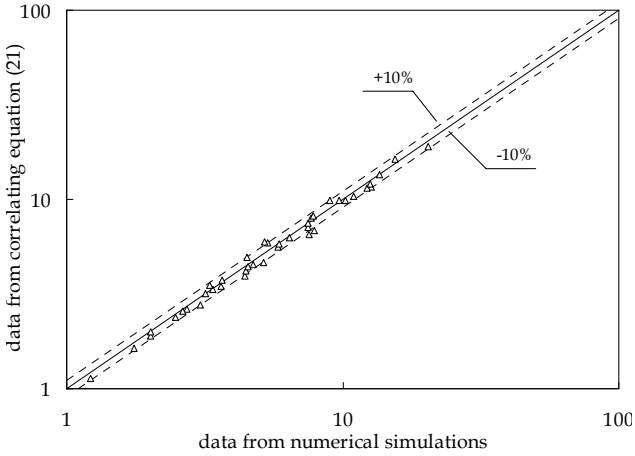

Figure 13 –Nu* from eq. (21) vs. Nu* from numerical simulations

k thermal conductivity of the fluid
L length of the heated portion of the bottom endwall
Nu average Nusselt number based on H = hH/k
Nu* average Nusselt number based on L = hL/k
P dimensionless pressure
p pressure
Pr Prandtl number = ν/α
Q heat transfer rate
Ra Rayleigh number based on the cavity height = $= g\beta(T_H - T_C)H^3Pr/\nu^2$
Ra_L Rayleigh number based on the length of the heated portion of the bottom endwall = $g\beta(T_H - T_C)L^3Pr/\nu^2$
T temperature
T_0 reference temperature
t time
U dimensionless horizontal velocity component
V dimensionless vertical velocity component
u horizontal velocity component
v vertical velocity component
X dimensionless horizontal coordinate
Y dimensionless vertical coordinate
x horizontal coordinate
y vertical coordinate

W width of the enclosure

Greek symbols

α thermal diffusivity of the fluid
β coefficient of volumetric thermal expansion of the fluid
ν kinematic viscosity of the fluid
θ dimensionless temperature
ρ density of the fluid
ψ dimensionless stream function

Subscripts

av average value
C cold
H hot
max maximum value
0 at the reference temperature, at the heated wall

REFERENCES

[1] I. Sezai and A.A. Mohamad, Natural convection from a discrete heat source on the bottom of a horizontal enclosure, Int. J. Heat Mass Transfer 43 (2000) 2257-2266.

[2] O. Aydin and W. J. Yang, Natural convection in enclosures with localized heating from below and symmetrical cooling from sides, Int. J. Num. Meth. Heat Fluid Flow 10 (2000) 518-529.

[3] Q.H. Deng, G. F. Tang and Y. Li, A combined temperature scale for analyzing natural convection in rectangular enclosures with discrete wall heat sources, Int. J. Heat Mass Transfer 45 (2002) 3437-3446.

[4] B. Calcagni, F. Marsili and M. Paroncini, Natural convective heat transfer in square enclosures heated from below, Applied Thermal Engineering 25 (2005) 2522-2531.

[5] P.H. Oosthuizen and J.T. Paul, Natural convection in a rectangular enclosure with two heated sections on the lower surface, Int. J. Heat Fluid Flow 26 (2005) 587-596.

[6] J.P. Van Doormaal and G.D. Raithby, Enhancements of the simple method for predicting incompressible fluid flows, Numer. Heat Transfer 11 (1984) 147-163.

[7] B. P. Leonard, A stable and accurate convective modelling procedure based on quadratic upstream interpolation, Comp. Meth. in Appl. Mech. Engng. 19 (1979) 59-78.

[8] G. de Vahl Davis, Natural convection of air in a square cavity: a bench mark numerical solution, Int. J. Num. Meth. Fluids 3 (1983) 249–264.

[9] H. S. Mahdi and R. B. Kinney, Time-dependent natural convection in a square cavity: application of a new finite volume method, Int. J. Num. Meth. Fluids 11 (1990) 57–86.

[10] M. Hortmann, M. Peric and G. Scheuerer, Finite volume multigrid prediction of laminar natural convection: bench-mark solutions, Int. J. Num. Meth. Fluids 11 (1990) 189–207.